Measuring Photosynthetically Active Radiation with a Multi-Channel Integrated Spectral Sensor

Walter D. Leon-Salas, Jegan Rajendran
School of Engineering Technology
Purdue University
Indiana, USA
Email: wleonsal@purdue.edu

Miguel A. Vizcardo, Mauricio Postigo-Malaga
Universidad Nacional de San Agustin
Arequipa, Peru

2021 IEEE International Symposium on Circuits and Systems (ISCAS) | 978-1-7281-9201-7/20/$31.00 ©2021 IEEE | DOI: 10.1109/ISCAS51556.2021.9401321

***Abstract*—This paper presents a photosynthetically active radiation (PAR) sensor based on an 18-band spectral sensor chipset with integrated optical filters. PAR sensors are an important tool for farmers and the proposed solution offers a path to low-cost PAR sensors. A technique for correcting the optical spectral leakage in the spectral sensor chipset is proposed and is applied to measurements collected indoors and outdoors. Tests results show that the proposed sensor and leakage-correction technique outperform lab-grade commercially-available PAR sensors.**

I. Introduction

Photosynthetically active radiation (PAR) is defined as the electromagnetic radiation that stimulates the photosynthesis process in plants [1]. Measuring PAR is an important task in farming [2], in optimizing controlled environments such as greenhouses and urban agriculture sites [3], in plant biology [4] and in estimating energy generation from biomass [5,6].

High-end quantum PAR sensors are commercially available from a variety of vendors [7]–[12]. These sensors typically require a separate display or a datalogging unit for measurement visualization and storage. Although high-end PAR sensors might be too expensive for low-income farmers in developing countries, they are well suited for research labs and come hermetically enclosed for operation in a variety of environments. There have been several efforts to develop low-cost quantum PAR sensors reported in the literature [13]–[22]. Most of these sensors use silicon photodiodes due to their low cost and their good spectral responsivity in the 400 to 700 nm wavelength range. PAR sensors using GaAsP photodiodes and selenium photocells have also been explored [18]–[20]. The photodiode or photocell is outfitted with a bandpass optical filter with transmission in the PAR wavelength range. In [21], light-emitting diodes (LEDs) were used as wavelength-selective photo-sensors. This approach used blue and red LEDs operating in the photo-galvanic region and although these LEDs did not have a spectral response that matched exactly with the PAR spectrum, their combined outputs had good correlation with the output of lab-grade PAR sensors.

In this work we report the design and evaluation of a PAR sensor based on the AS7265x integrated spectral sensor from AMS [23]. The AS7265x sensor is a three-chip light sensing solution featuring 18 spectral channels covering the 410 nm to 940 nm spectral range. The advantages of the proposed PAR sensor include improved accuracy, the ability to provide spectral information of a light source (in addition to PAR measurements), low cost (∼$5 per chip) and its capacity to measure near infrared (NIR) radiation, a useful feature when assessing the effectiveness of NIR filtering in greenhouses [24]. This paper proposes a method based on vector quantization to calibrate the proposed PAR sensor and correct for its internal spectral leakage. Test results and performance assessment are reported.

II. Background

A. Photosynthetically Active Radiation

Photosynthesis is a biochemical process, driven by radiant energy, in which glucose is synthesized from carbon dioxide and water. In plants, photosynthesis occurs primarily in leaves in organelles called chloroplasts. It has been shown that radiation of different wavelengths stimulates photosynthesis at different rates [25]. Furthermore, McCree established that only radiation within the 360 to 760 nm wavelength range has the potential to drive photosynthesis [26]. A common and practical approach for measuring PAR restricts the wavelength range of the incident radiation from 400 to 700 nm. This restriction is adopted because the contribution of light outside this range to the photosynthetic process is minimal. In order to simplify measurements, each wavelength within this ranage is assigned equal weight. This simplification is based on the Stark-Einstein principle, which states that one absorbed photon excites one electron regardless of the photon's energy or wavelength [27]. PAR sensors that assign equal weight to photons in the 400 to 700 nm range are said to measure the photosynthetic photon flux density (PPFD) and are commonly called quantum PAR sensors.

Given the spectral irradiance I_λ, defined as the radiant flux per unit wavelength and unit area, the photon flux density in the PAR wavelength range can be calculated using the following expression:

$$\phi = \int_{400}^{700} \frac{I_\lambda \, d\lambda}{E_{ph}(\lambda)} \tag{1}$$

where, $E_{ph}(\lambda) = hc/\lambda$ is the energy of a photon of wavelength λ, h is Plank's constant and c is the speed of light.

The PPFD is simply the photon density flux measured in units of micro-moles of photons per square meter per second (μmol m^{-2} s^{-1}), where a mole of photons is defined as $N_A = 6.022 \times 10^{23}$ (Avogadro's number) photons. Hence, the PPFD (or Q_{PAR}) can be calculated as follows:

$$Q_{PAR} = \frac{\phi}{N_A \times 10^6} \tag{2}$$

Combining (1) and (2), yields the following expression for the PPFD:

$$Q_{PAR} = \left(\frac{10^{-6}}{hcN_A}\right) \int_{400}^{700} \lambda \; I_\lambda(\lambda) \; d\lambda \tag{3}$$

As shown in equation (3), the PPFD can be directly calculated from the spectral irradiance. Measuring the spectral irradiance requires the use of an spectroradiometer. Spectroradiometers are calibrated precision optical instruments and are an expensive solution for measuring PAR, especially for farming applications where a low-cost and portable solution would be preferable. Most commercially-available quantum PAR sensors use a single photo-detector and an optical filter stack to approximate the integral in (3).

B. Integrated Spectral Sensor

The AS7265x spectral sensing solution consists of three integrated circuits (ICs): AS72651, AS72652 and AS72653. Each IC contains six optical channels for a total of 18 channels covering the 410 nm to 940 nm spectral range. Each channel features an optical Gaussian filter with a full width half maximum (FWHM) bandwidth of 20 nm. The distribution of the optical channels across the three ICs is shown in Fig. 1 (a). The gain and the integration time of the optical channels is configurable via internal registers. A 16-bit analog-to-digital converter (ADC) in each IC converts the output of the optical channels to digital. Because the AS7265x sensor is able to provide spectral information about a light source, it has the potential to be an accurate PAR sensor. Another attractive feature of the AS7265x sensors is their low cost, with each IC costing around 5 USD.

Fig. 1 (b) shows the normalized response of the optical filters. This figure conceptually shows a non-ideal response of the optical filters known as spectral leakage. Due to spectral leakage, NIR radiation induces an output on optical channels that should not respond to NIR. To alleviate this problem, a NIR-blocking optical filter could be placed on top of the sensor. However, this will increase costs and would preclude the sensor from providing NIR information, information which could be a useful in some applications [24]. In this work a calibration method based on vector quantization is used to correct for spectral leakage without the need of additional optical filters.

III. Proposed PAR Sensor

Fig. 2 shows a diagram of the proposed PAR sensor. The sensor is based on the AS7265x evaluation kit from AMS [29]. This kit includes a printed circuit board with the three

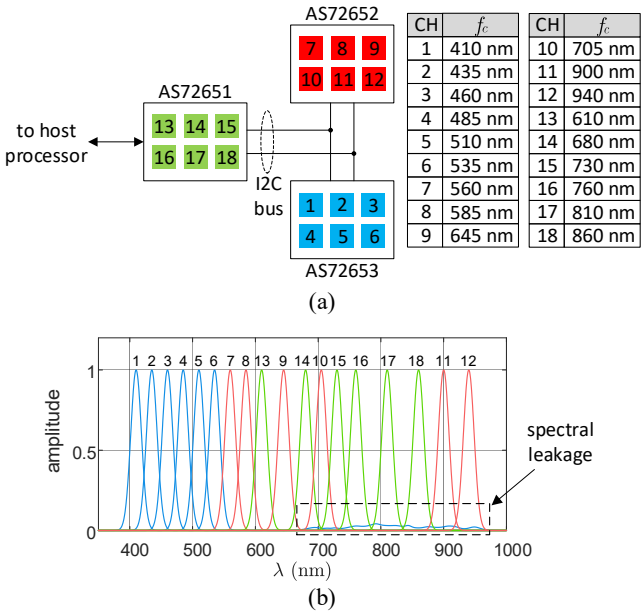

CH	f_c	CH	f_c
1	410 nm	10	705 nm
2	435 nm	11	900 nm
3	460 nm	12	940 nm
4	485 nm	13	610 nm
5	510 nm	14	680 nm
6	535 nm	15	730 nm
7	560 nm	16	760 nm
8	585 nm	17	810 nm
9	645 nm	18	860 nm

Fig. 1: Spectral sensor AS7265x. (a) simplified schematic diagram showing inter-chip connectivity and distribution of optical channels; (b) normalized optical filter response.

spectral sensor ICs, a plastic enclosure and a light diffuser. The optical path of the AS7265x sensors is optimized for diffuse light, hence, a light diffuser is needed to be able to work with direct non-diffuse light. Data from the AS7265x ICs is read serially by a micro-controller board (Arduino Uno) and sent to a personal computer for storage and analysis. Data retrieved from the AS7265x ICs is a set of 18 16-bit unsigned integers.

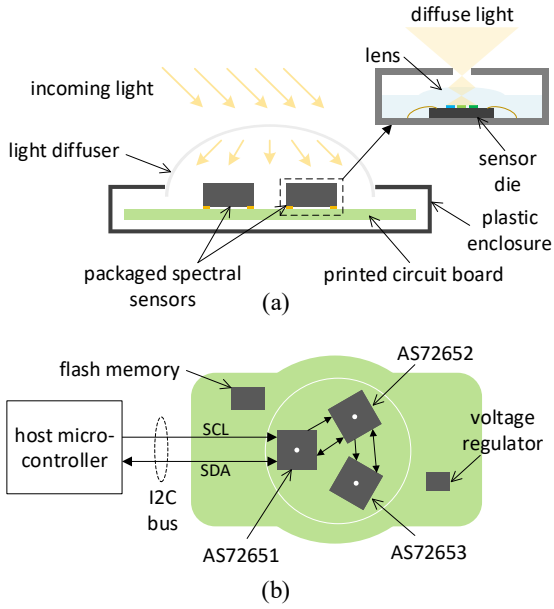

Fig. 2: Diagram of the proposed AS7265x-based PAR sensor. (a) cross-sectional view; (b) top view.

A. Sensor Calibration Approach

The raw data read from the AS7265x ICs is first normalized by dividing it by the gain and the integration time of the optical channels. This normalized output is stored in vector Y and is said to have units of basic counts. The vector Y is a function of the photon flux in each optical channel plus spectral leakage due to the non-ideal response of the optical filters. Let $X = [x_1, x_2, \cdots, x_i, \cdots x_{18}]$ be the filtered photon flux vector in which each vector element x_i is defined as:

$$x_i = \int \frac{f_i(\lambda) \cdot I_\lambda}{E_{ph}(\lambda)} d\lambda \tag{4}$$

where, $f_i(\lambda)$ is the response of the i^{th} optical filter and $i = 1, 2, \cdots 18$. Figs. 3 and 4 show the vectors X and Y along with the measured spectral irradiance I_λ for a fluorescent lamp and for solar light, respectively. The spectral irradiances were measured with a calibrated spectroradiometer (BlackComet from StellarNet). Since the fluorescent lamp does not emit significant NIR radiation, spectral leakage is not manifested and the normalized sensor output Y follows the filtered photon flux X. However, when the spectral sensor is illuminated by the sun, which emits much higher levels of NIR radiation, the spectral sensor output is noticeably affected.

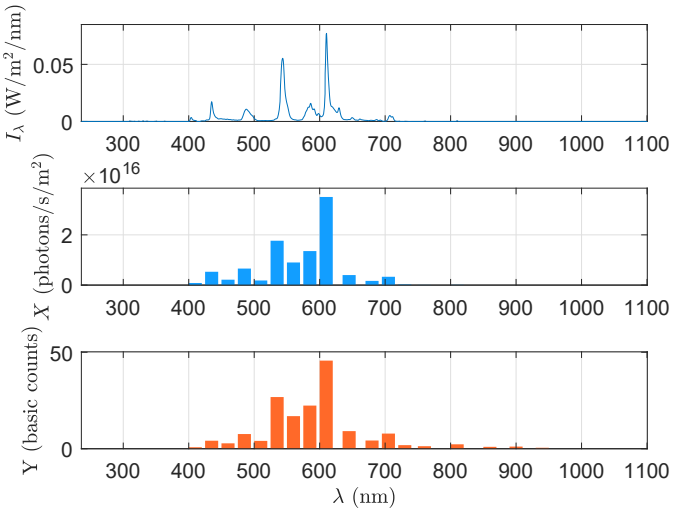

Fig. 3: Comparison between spectral irradiance, filtered photon flux X and normalized sensor output Y for a fluorescent lamp.

In order to correct for spectral leakage and calibrate the spectral sensor, a method based on vector quantization was implemented. This method has a training phase and a correction phase. In the training phase, M spectral measurements spanning several light sources and lighting conditions are collected using the AS7265x spectral sensor and the BlackComet spectroradiometer. A pseudo-code outlining the steps carried out in the training phase is shown in Algorithm 1.

In this pseudo-code the function $\texttt{kmeans}(V_m^i, K)$ clusters the set of vectors V_m^i for optical channel i into K clusters using the k-means algorithm. The function returns the centroids C_k^i of each cluster. Each centroid is a 19-element vector,

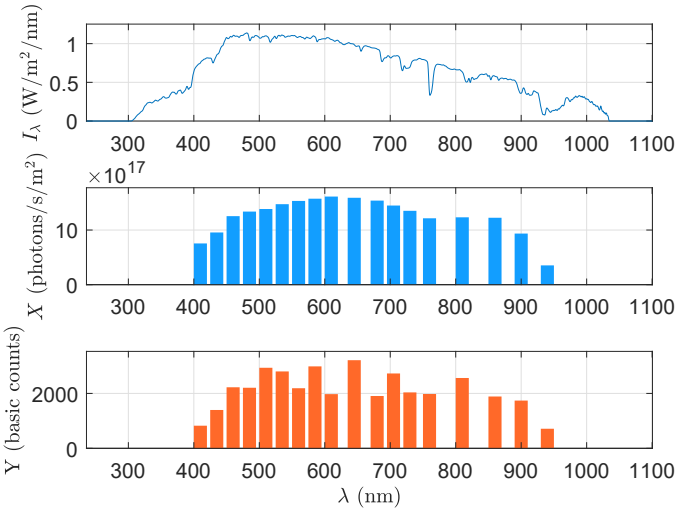

Fig. 4: Comparison between spectral irradiance, filtered photon flux X and normalized sensor output Y for solar light on a sunny afternoon.

$m = 1$;
while $m \leq M$ **do**
  acquire $Y = [y_1, y_2, \cdots y_{18}]$;
  measure I_λ;
  calculate $X = [x_1, x_2, \cdots x_{18}]$ using (4);
  calculate $h_i = x_i / y_i$ for $i = 1, 2, \cdots 18$;
  set $V_m^i = [Y, h_i]$ for $i = 1, 2, \cdots 18$;
  $m = m + 1$;
end
$\{C_k^i\}$ = $\texttt{kmeans}(V_m^i, K)$, $i = 1, \cdots 18$, $k = 1, \cdots K$;

Algorithm 1: Pseudo-code for the training phase.

i.e. $C_k^i = [c_{1,k}^i, c_{2,k}^i, \cdots c_{18,k}^i, c_{19,k}^i]$. The pseudo-code for the correction phase is shown in Algorithm 2. The correction phase starts by acquring a new normalized measurement, Y, from the spectral sensor, it then finds the centroid that is the closest to Y and uses the last element in that centroid, $c_{19,k}^i$, as a correction factor to calculate the estimated filtered photon flux vector $\widehat{X} = [\widehat{x}_1, \widehat{x}_2, \cdots \widehat{x}_{18}]$. Linear interpolation is then used to estimate the value of $\widehat{X}$ at 628 nm and 663 nm, which are spectral bands missing in the spectral sensor (see Fig. 1). The value of PAR is obtained by adding up the elements in $\widehat{X}$ and multiplying the result by a scaling factor.

IV. Results

In order to calibrate the proposed PAR sensor, a training data set consisting of 24 spectral measurements was collected using the AS7265x spectral sensor and a calibrated BlackComet spectroradiometer. This training data set includes spectra from a full-spectrum LED-based light for indoor plant grow with variable intensity [30] and outdoor measurements under the following conditions: direct light on a clear day (morning, afternoon and sunset), cloudy sky (morning and afternoon), under the shade of a building and under a tree canopy.

acquire $Y = [y_1, y_2, \cdots y_{18}]$;
for $i = 1$ **to** 18 **by** 1 **do**
  $d_{min} = \|Y\|_2$;
  for $k = 1$ **to** K **by** 1 **do**
    $\widetilde{Y} = [c^i_{1,k}, c^i_{2,k}, \cdots c^i_{18,k}]$;
    $d_k = \|Y - \widetilde{Y}\|_2$;
    if $d_k < d_{min}$ **then**
      $d_k = d_{min}$; $\widehat{h_i} = c^i_{19,k}$;
    end
  end
  $\widehat{x_i} = \widehat{h_i} \times y_i$;
end

Algorithm 2: Pseudo-code for the correction phase.

Measurements from the full-spectrum LED light at 11 different intensities were collected. Fig. 5 shows the setup used to collect measurements from this light source. The calibration algorithm was implemented in MATLAB and took 0.5 sec. to run on a Windows 10 laptop with an i7 processor.

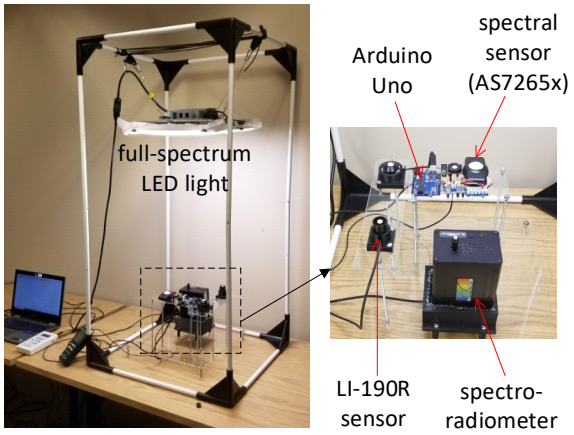

Fig. 5: Setup employed to acquire training data for calibration of the spectral sensor.

For the correction phase we collected measurements from light sources that were not included in the training phase such as fluorescent, atrium and a red-green-blue (RGB) programmable LED light. We also collected measurements outdoors in conditions similar to the ones used in the training phase but in different locations and on different days. Fig. 6 shows some of the light sources and locations used in the correction phase. Table I lists PAR values: 1) calculated using equation (3) and the measured spectral irradiance I_λ, 2) calculated from the estimated filtered photon flux vector $\widehat{X}$ and 3) measured with a lab-grade commercially-available quantum PAR sensor (LI-190R from LI-COR). The table also shows the error with respect to the PAR calculated from I_λ.

V. Conclusion

A PAR sensor based on the 18-band AS7265x spectral sensor chipset has been presented. A technique for correcting the optical spectral leakage in the AS7265x sensor was described and applied to measurements collected indoors and outdoors. An average error of 6.83%, with respect to reference PAR values calculated using a calibrated spectroradiometer, was obtained using this technique. A 12.51% average error was obtained with a commercially-available PAR sensor under the same conditions. This result validates the proposed sensor architecture and calibration method. Future work includes tests with larger data sets and with sensor ICs from different fabrication lots.

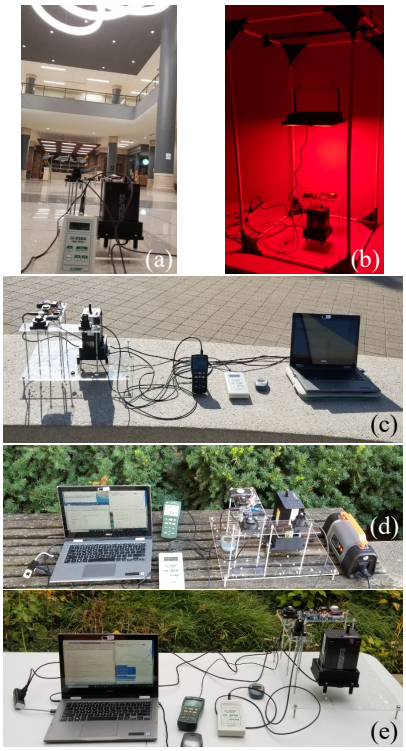

Fig. 6: Correction phase locations. (a) building atrium; (b) RGB LED; (c) outdoor sunny; (d) under shade; (e) cloudy.

TABLE I: **Correction Phase Results**

light source	PAR from I_λ $\left(\frac{\mu mol}{s \cdot m^2}\right)$	from $\widehat{X}$ PAR $\left(\frac{\mu mol}{s \cdot m^2}\right)$	from $\widehat{X}$ error (%)	LI-190R PAR $\left(\frac{\mu mol}{s \cdot m^2}\right)$	LI-190R error (%)
fluorescent	8.472	8.925	5.35	8.08	4.63
building atrium	5.915	6.279	6.16	4.41	25.44
RBG LED (white)	24.388	22.077	9.48	21.27	12.79
RBG LED (red)	16.365	15.704	4.04	14.88	9.07
RBG LED (green)	15.686	14.321	8.70	14.02	10.62
RBG LED (blue)	25.618	21.072	17.74	21.00	18.03
sunny morning	781.332	763.916	2.23	726.7	6.99
sunny afternoon	1385.07	1486.18	7.30	1197.0	13.58
cloudy morning	50.690	51.588	1.77	43.94	13.31
under shade	45.909	48.471	5.58	41.04	10.61
average error			**6.83**		12.51

Acknowledgement

The authors would like to thank to Universidad Nacional de San Agustin of Arequipa, Peru for their financial support.

REFERENCES

[1] I. Alados, I. Foyo-Moreno and L. Alados-Arboledas, "Photosynthetically active radiation: measurements and modelling," *Agricultural and Forest Metereology*, no. 78, pp. 121-131, 1996.

[2] G. Grigera, M. Oesterheld and F. Pacon, "Monitoring forage production for farmers' decision making," *Agricultural Systems*, vol. 94, no. 3, pp. 637-648, 2007.

[3] J. G. Pieters and J. M. Deltour, "Modelling solar energy input in greenhouses," *Solar Energy*, vol. 67, no. 1-3, pp. 119-130, 1999.

[4] G. Ries, G. Buchholz, H. Frohnmeyer and B. Hohn, "UV-damage-mediated induction of homologous recombination in *Arabidopsis* is dependent on photosynthetically active radiation," *Proc. National Academy of Sciences*, vol. 97, no. 24, pp. 13425-13429, 2000.

[5] E. Habyarimana, I. Piccard, M. Catellani, P. De Franceschi and M. Dall'Agata, "Towards predictive modeling of sorghum biomass yields using fraction of absorbed photosynthetically active radiation derived from sentinel-2 satellite imagery and supervised machine learning techniques", *Agronomy*, vol. 9, no. 4, pp. 203, 2019.

[6] X.-G. Zhu, S. P. Long and D. R. Ort, "What is the maximum efficiency with which photosynthesis can convert solar energy into biomass?," *Current Opinion in Biology*, vol. 19, no. 2, pp. 153-159, 2008.

[7] LI-COR, *LI-COR light measurements*. Accessed on: Oct. 18, 2020. [Online]. Available: https://www.licor.com/env/products/light/.

[8] Apogee, *Quantum sensors - PAR meters*. Accessed on: Oct. 18, 2020. [Online]. Available: https://www.apogeeinstruments.com/quantum/.

[9] Kippzonen, *PQS1 PAR Quantum Sensor*. Accessed on: Oct. 18, 2020. [Online]. Available: https://www.kippzonen.com/Product/184/PQS1-PAR-Quantum-Sensor#.X4yFOhKSlPY.

[10] Hansatech, *QSPAR Quantum Sensor*. Accessed on: Oct. 18, 2020. [Online]. Available: http://www.hansatech-instruments.com/product/qspar-quantum-sensor/.

[11] Hydrometeorologische Instrumente und Messanlagen, *PAR Sensor 0... 100 mV*. Accessed on: Oct. 18, 2020. [Online]. Available: https://www.meteorologyshop.eu/sensoren/strahlungssensoren/par/553/par-sensor-0-100-mv.

[12] Hydrometeorologische Instrumente und Messanlagen, *ML-020P PAR Sensor*. Accessed on: Oct. 18, 2020. [Online]. Available: https://eko-eu.com/products/environmental-science/small-sensors/ml-020p-par-sensor.

[13] D. Yadav, M. A. Sumesh, T. Beno, S. P. Karanth, and G. Sadashivappa. "Design of Photosynthetically Active Radiation Sensor," *Examines in Physical Medicine and Rehabilitation*, vol. 1, no. 5, 2018.

[14] M. V. C. Caya, J. T. Alcantara, J. S. Carlos and Sherwin S. B. Cereno, "Photosynthetically active radiation (PAR) sensor using an array of light sensors with the integration of data logging for agricultural application," *International Conference on Computer and Communication Systems (ICCCS)*, pp. 377-381, 2018.

[15] H. R. Barnard, M. C. Findley, J. Csavina, "PARduino: A simple and inexpensive device for logging photosynthetically active radiation," *Tree Physiology*, vol. 34, no. 6, pp. 640-645, 2014.

[16] C. R. Booth, "The design and evaluation of a measurement system for photosynthetically active quantum scalar irradiance," *Limnology and Oceanography*, vol. 21, no. 2, pp. 326-336, 1976.

[17] F. I. Woodward, "Instruments for the measurement of photosynthetically active radiation and red, far-red and blue light," *Journal of Applied Ecology*, vol. 20, pp. 103-115, 1983.

[18] P. Fielder and P. G. Comeau, "Construction and testing of an inexpensive PAR sensor," Ministry of Forests Research Program, vol. 53, British Columbia, 2000.

[19] R. C. Muchow and G. L. Kerven, "A low cost instrument for measurement of photosynthetically active radiation in field canopies," *Agricultural Meteorology*, vol. 18, no. 3, pp. 187-195, 1977.

[20] K. J. McCree, "A solarimeter for measuring photosynthetically active radiation," *Agricultural Meteorology*, vol. 3, no. 5-6, pp. 353-366, 1966.

[21] F. Mims III, "A 5-year study of a new kind of photosynthetically active radiation sensor," *Photochemistry and Photobiology*, vol. 77, no. 1, pp. 30-33, 2003.

[22] J. Rajendran, W. D. Leon-Salas, X. Fan, Y. Zhang, M. A. Vizcardo, and M. Postigo, "On the Development of a Low-Cost Photosynthetically Active Radiation (PAR) Sensor," *IEEE International Symposium on Circuits and Systems*, pp. 1-5, 2020.

[23] ams, *AS7265x Smart Spectral Sensor*. Accessed on: Oct. 20, 2020. [Online]. Available: https://ams.com/as7265x.

[24] S. Hemming, F. Kempkes, N. van der Braak, T. Dueck, and N. Marissen, "Greenhouse cooling by NIR-reflection," *International Symposium on Greenhouse Cooling*, vol. 719, pp. 97-106, 2006.

[25] K. Inada, "Action spectra for photosynthesis in higher plants," *Plant Cell Physiology*, vol. 17, pp. 355-365, 1976.

[26] K. J. McCree, "The action spectrum, absorptance and quantum yield of photosynthesis in crop plants," *Agricultural Metereology*, vol. 9, pp. 191-216, 1970.

[27] C. Barnes, T. Tibbitts, J. Sager, G. Deitzer, D. Bubenheim, G. Koerner and B. Bugbee, "Accuracy of quantum sensors measuring yield photon flux and photosynthetic photon flux," *Horticultural Science*, vol. 28, no. 12, pp. 1197-1200, 1996.

[28] M. Mõttus, M. Sulev, F. Baret, R. Lopez-Lozano and A. Reinart, "Photosynthetically active radiation: measurement and modeling," *Encyclopedia of Sustainability Science and Technology*, pp. 7902-7932, 2012.

[29] ams, *Demo Kit for AS7265x*. Accessed on: Oct. 28, 2020. [Online]. Available: https://ams.com/as7265xdemokit.

[30] Mars Hydro, *Mars Hydro TS 1000 LED grow light for indoor plants full spectrum 150W 2ftx2ft 3ftx3ft coverage*. Accessed on: Nov. 3, 2020. [Online]. Available: https://www.mars-hydro.com/hpcall/new-arrivel-hp/mars-ts-1000-led-full-spectrum-hydroponic-led-grow-light